



Hydrothermal synthesis of defective TiO₂ nanoparticles for long-wavelength visible light-photocatalytic killing of cancer cells

| | |
|-------------------------------|---|
| Journal: | <i>RSC Advances</i> |
| Manuscript ID | RA-ART-09-2015-019045.R1 |
| Article Type: | Paper |
| Date Submitted by the Author: | 23-Oct-2015 |
| Complete List of Authors: | Lee, Jooran; Korea Basic Science Institute (KBSI), Division of scientific instrumentation Lee, Young Hwa; Chungnam National University, Department of Biochemistry Choi, Joon Sig; Chungnam National University, Department of Biochemistry Park, Kwan Seob; Korea Basic Science Institute (KBSI), Division of scientific instrumentation Chang, Ki Soo; Korea Basic Science Institute (KBSI), Division of scientific instrumentation Yoon, Minjoong; Chungnam National University, Department of Chemistry |
| Subject area & keyword: | Nanomedicine < Nanoscience |
| | |



Journal Name

ARTICLE

Hydrothermal synthesis of defective TiO₂ nanoparticles for long-wavelength visible light-photocatalytic killing of cancer cells

Jooran Lee^{a,c}, Young Hwa Lee^b, Joon Sig Choi^b, Kwan Seob Park^c, Ki Soo Chang^{c*} and Minjoong Yoon^{a,d*}

Received 00th January 20xx,
Accepted 00th January 20xx

DOI: 10.1039/x0xx00000x

www.rsc.org/

Defective TiO₂ nanoparticles (*d*-TiO₂ NPs) were successfully synthesized using a simple hydrothermal technique through the formation of liposome-TiO₂ composites using P25 TiO₂ powder as the starting material. The morphology and vibrational structures of the *d*-TiO₂ NPs were characterized by various techniques, including X-ray diffraction, transmission electron microscopy, and Fourier transform-infrared and Raman spectroscopic analyses. The synthesized *d*-TiO₂ NPs were composed of both the rutile and anatase phases of TiO₂ with a diameter of approximately 25 nm, and they exhibited absorption of broad visible light including near-infrared wavelengths, from 400 nm to 1000 nm, which was confirmed by diffuse reflectance spectroscopy and X-ray photoelectron spectroscopy. The agglomeration size of the *d*-TiO₂ NPs in aqueous solution was lesser (224 nm) than that of P25 TiO₂ (1440 nm). Therefore, the synthesized *d*-TiO₂ NPs could more easily infiltrate the membrane and cytoplasm of cancer cells *via* endocytosis than could P25 TiO₂. Consequently, upon irradiation with long-wavelength visible light (400–800 nm), the *d*-TiO₂ NPs could generate reactive oxygen species, including singlet oxygen, leading to the destruction of cancer cells. These results suggest that the newly fabricated *d*-TiO₂ NPs are promising nanomaterials for future *in vivo* photodynamic therapy of cancer.

Introduction

In the past decade, the use of various semiconductor nanomaterials in biomedicine has increased owing to their controllable size, shape, and dimensionality, making them suitable for several applications, including biosensing, cell imaging, drug/gene delivery and cancer therapy.^{1–4} In particular, TiO₂ nanoparticles (NPs) show advantages of strong photocatalytic activity, non-toxicity, high photostability, and low cost, and have thus attracted much attention as alternative phototherapy (PDT) agents^{5–10} to replace conventional dye sensitizers such as porphyrin derivatives.¹¹ The majority of pristine TiO₂ NPs are active under ultraviolet (UV) light excitation due to their large band gap energy (~3.2 eV). However, UV light induces damage to biological components, and its penetration into a biological tissue is very limited; thus, UV light is often unable to reach the cancer cells located far from the tissue surface. Consequently, UV-sensitive TiO₂ NPs are not useful for successful *in vivo* PDT, which requires long-wavelength visible-light or near-infrared (NIR) irradiation. Thus, TiO₂ NPs have been modified by doping carbon, nitrogen,^{12–14} and some transition metals,^{15–17} which can narrow their band gap energies and in turn enhance

their photoactivity under visible-light excitation. Nevertheless, the doping materials may have adverse effects on biomolecules due to their toxicity, and the doped TiO₂ NPs absorb only a short range of visible light (400–600 nm), which has limited penetration distance in the tissue. The NIR range (700 ~1000 nm) light shows the maximum penetration of light into tissues.¹⁸ In addition to light responses, determining the appropriate size and morphologies of TiO₂ NPs is an important prerequisite for their efficient infiltration into biological cells,¹⁹ because conventional TiO₂ NPs are easily aggregated in an aqueous environment. Thus, it is necessary to develop longer-wavelength visible light (up to the NIR range)-sensitive TiO₂ NPs with minimum aggregation, biocompatibility, and non-toxicity.

In recent years, many researchers have attempted a defect-engineering method with an electron beam (EB) to avoid the use of hazardous dopants.^{20–22} EB irradiations have been applied to form TiO₂ NPs containing defect sites such as oxygen vacancies, which can lead to the creation of unpaired electrons or Ti³⁺ centers. These Ti³⁺ defects can form a shallow donor level just below the conduction band, which could facilitate both visible light and NIR responses.^{23–24} Thus, owing to efficient interfacial electron transfer, EB-generated defective TiO₂ NPs (*d*-TiO₂ NPs) have been successfully applied to induce visible light-driven photocatalytic activity for water splitting and CO₂ reduction.²¹ However, *d*-TiO₂ NPs have not yet been employed for biomedical applications such as PDT. Further, the EB technique requires the use of a high-energy EB accelerator under high-vacuum conditions, which makes it a costly procedure. Hereby, we developed a simple method for the hydrothermal synthesis of *d*-TiO₂ NPs through the formation of liposome-TiO₂ nanocomposites, and investigated their optical and structural properties for exploring their photocatalytic effects on the viability of cancer cells²⁵ under visible light irradiation.

^a Molecular/Nano Photochemistry and Photonics Lab, Department of Chemistry, Chungnam National University, Daejeon 305-764, South Korea.

^b Department of Biochemistry, College of Natural Sciences, Chungnam National University, Daejeon 305-764, South Korea.

^c Division of Scientific Instrumentation, Korea Basic Science Institute, Daejeon 305-806, South Korea.

^d KD Chemical-JNT, Inc. Ltd., Moonpyung-dong, Daedeok-gu, Daejeon 306-220, South Korea.

†Electronic Supplementary Information (ESI) available: Additional data of diffuse reflectance absorption spectra, zeta potential and particle size measurements. See DOI: 10.1039/x0xx00000x

*These authors are co-corresponding authors.

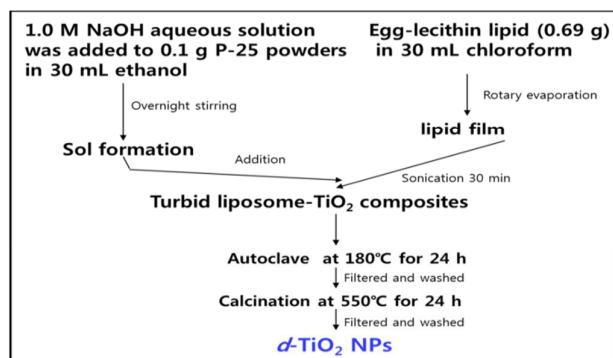


Fig. 1 Schematic flow chart for the synthesis of *d*-TiO₂ NPs

Results and discussion

Structural and optical properties

Fig. 2 (A) shows the XRD pattern of the as-synthesized *d*-TiO₂ NPs, which exhibited the same pattern as that of P25 TiO₂ and EB-induced *d*-TiO₂ NPs. This indicates that these *d*-TiO₂ NPs possess a mixture of both the rutile and anatase phases.^{20,30} The XRD intensities of the *d*-TiO₂ NPs slightly decreased compared to those of P25 TiO₂, indicating that the defects and surface modification of the *d*-TiO₂ NPs reduced the crystallinity.²⁰ The average crystallite size of the NPs was calculated using the Scherrer equation, $D = k\lambda / \beta \cos\theta$, where k is the shape factor of the particles and has a typical value of 0.89, λ is the wavelength of the X-ray (1.5406 Å), β is the peak broadening in radians (full width at half maximum; FWHM), and θ is the Bragg angle.³¹ The average particle sizes of the anatase phase obtained using this formula were approximately 18.2 nm (*d*-TiO₂ NPs) and 17.5 nm (P25 TiO₂), and the average crystallite sizes of the rutile phase were approximately 27.0 nm (*d*-TiO₂ NPs) and 24.6 nm (P25 TiO₂). The increase in the particle size under the hydrothermal reaction confirmed the transformation of the phase and defects at the surface of the TiO₂ NPs.^{20,32}

In order to confirm the surface defects, vibrational structures of the *d*-TiO₂ NPs were evaluated by Raman spectroscopy. In general, there are six (144 cm⁻¹ (E_g), 197 cm⁻¹ (E_g), 397 cm⁻¹ (B_{1g}), 518 cm⁻¹ (A_{1g} + B_{1g}), 640 cm⁻¹ (E_g)) and four (144 cm⁻¹ (B_{1g}), 488 cm⁻¹ (E_g), 613 cm⁻¹ (A_{1g}), 827 cm⁻¹ (B_{2g})) Raman active modes for anatase and rutile TiO₂, respectively.³³ The *d*-TiO₂ NPs showed the typical Raman bands, although they were broader, as shown in Fig. 2 (B). The FWHM of the *d*-TiO₂ NPs and P25 TiO₂ were 9.57 and 8.34 cm⁻¹ at 144 cm⁻¹ (E_g), respectively. The broadening of the Raman peaks of the *d*-TiO₂ NPs indicates that various defects had formed, such as oxygen vacancies and Ti³⁺.²⁰

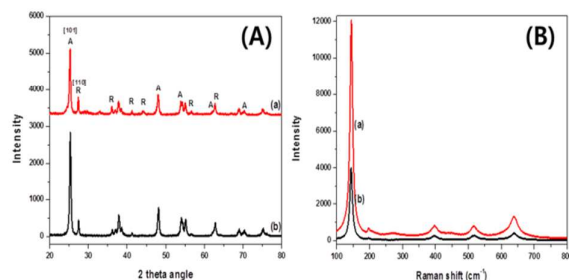


Fig. 2 X-ray diffraction pattern (A) and Raman spectra (B) of *d*-TiO₂ NPs (a) and P25 TiO₂ (b)

The FT-IR spectra of the *d*-TiO₂ NPs were recorded in KBr phase in the frequency region of 400–4000 cm⁻¹ (Fig. 3). The functional groups of the recorded FT-IR spectra were compared with the standard spectra of the TiO₂ NPs. The vibration bands observed at ~534 cm⁻¹ in all spectra were attributed to the vibration of the Ti-O bond in the TiO₂ lattice. The absorption bands at 1640 cm⁻¹ and 1500 cm⁻¹ were caused by the bending vibrations of Ti-O-H and Ti-O-Ti, respectively. Furthermore, a broad peak appearing at 3100–3600 cm⁻¹ caused by the fundamental stretching vibration of O-H hydroxyl groups reduced in the *d*-TiO₂ NPs. Moreover, additional vibrational bands were observed at 3746 and 3850 cm⁻¹, indicating the existence of octahedral (6Ti³⁺-OH) and tetrahedral (4Ti⁴⁺-OH) coordinated vacancies.^{34,35} These results indicate that the *d*-TiO₂ NPs have more oxygen vacancies than P25 TiO₂.

Further detailed structures, particle sizes, and structural characterization of the *d*-TiO₂ NPs were determined using field-emission TEM combined with the selected area electron diffraction (SAED) pattern. As shown in Fig. 4, the observed lattice spacing was approximately 0.35 nm, close to the anatase [101] planes.³⁶ The size distribution determined from the TEM image was similar to that calculated using the Scherrer equation, revealing that the particles size was in the range ~25 nm.

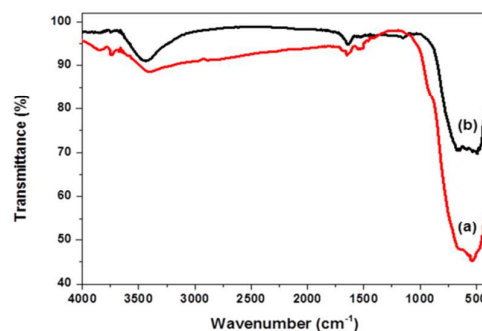


Fig. 3 FT-IR spectra of *d*-TiO₂ NPs (a) and P25 TiO₂ (b)

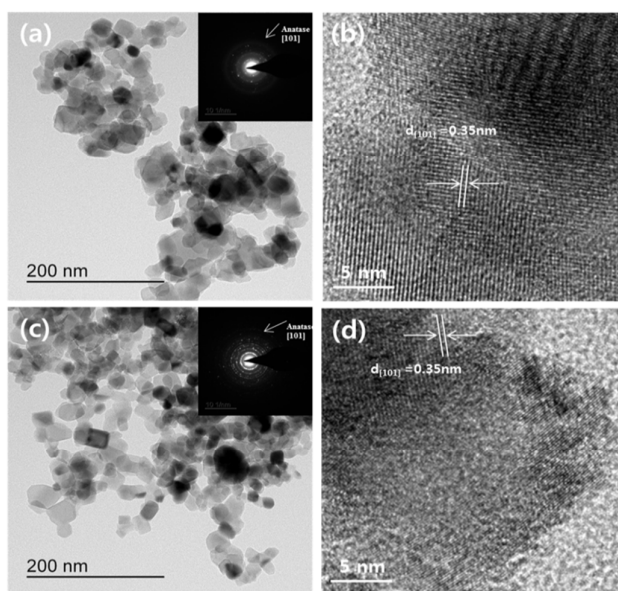


Fig. 4 TEM images of *d*-TiO₂ NPs (a) and P25 TiO₂ (c); HRTEM images of *d*-TiO₂ NPs (b) and P25 TiO₂ (d). The insets in (a) and (c) show the electron diffraction pattern of the corresponding selected area.

To investigate the optical properties of the *d*-TiO₂ NPs, the diffuse reflectance UV-visible absorption spectrum was measured at room

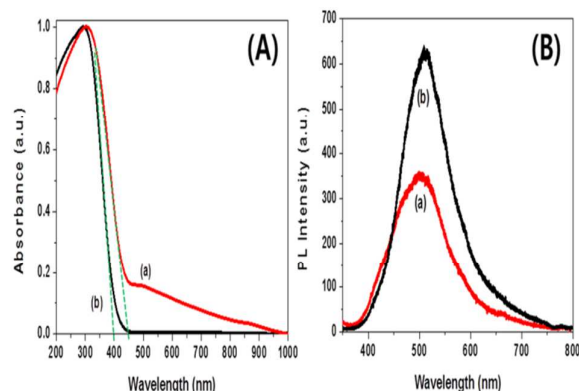


Fig. 5 UV-visible reflectance absorption spectra (A) and ensemble-averaged fluorescence spectra (B) of *d*-TiO₂ NPs (a) and P25 TiO₂ (b); the excitation wavelength was 325 nm.

temperature, as shown in Fig. 5(A). Compared with the absorption spectrum of P25 TiO₂ (curve b), the absorbance of the *d*-TiO₂ NPs (curve a) was higher in the broad-visible region from 400 nm up to the NIR range (700 - 1000 nm) due to the surface defects. The surface defects are formed through reaction of Ti³⁺ with a certain amount of oxygen under hydrothermal equilibrium condition,²⁶ and their optimum amount could be obtained at 180 °C as proved by the temperature dependence of the red-shifted absorption (Fig. S1). The band gap energies of *d*-TiO₂ NPs and P25 TiO₂ were 2.77 eV and 3.11 eV, respectively. This decrease in the band gap energy may be due to the localized surface states induced by Ti³⁺, which can form donor levels in the electronic structure of TiO₂, as well as the oxygen vacancies, which can affect the electron-hole (e-h) recombination process.^{20,34,37-38} The bulk defects only act as charge-carrier traps where e-h recombine, whereas the surface defects can also facilitate charge transfer to adsorbed species, which can prevent e-h recombination, as well as serve as charge-carrier traps.^{23,39} This speculation is supported by the observation that the fluorescence emission intensity of the *d*-TiO₂ NPs was quenched compared to that of P25 TiO₂ under the same excitation condition at 325 nm (Fig. 5(B)). This is likely due to the fact that *d*-TiO₂ NPs have more surface defects than P25 TiO₂. Thus, it is expected that the *d*-TiO₂ NPs would have higher photocatalytic activities under visible light radiation.

For further confirmation of the structural and defect properties, we analyzed the chemical bonding of TiO₂ NPs by XPS. Fig. 6 shows the XPS spectra of the Ti 2p_{3/2} and O 1s core levels recorded from *d*-TiO₂ NPs (spectra a and c) and P25 TiO₂ (spectra b and d). The Ti 2p_{3/2} and O 1s XPS peaks of the *d*-TiO₂ NPs were observed at 458.8 eV (Ti⁴⁺2p_{3/2}), 458.0 eV (Ti³⁺2p_{3/2}), 530.0 eV [TiO₂ (Ti⁴⁺)], 531.1 eV [Ti₂O₃ (Ti³⁺)], and 532.1 eV [water adsorbed on the TiO₂ surface].^{20,22,33} The XPS peaks of P25 TiO₂ were observed at 458.6 eV (Ti⁴⁺2p_{3/2}), 457.5 eV (Ti³⁺2p_{3/2}), 529.8 eV [TiO₂ (Ti⁴⁺)], 531.1 eV [Ti₂O₃ (Ti³⁺)], and 532.2 eV [water adsorbed on the TiO₂ surface]. The amount of Ti³⁺ on the TiO₂ surface plays an important role, as previously reported for TiO₂ doped with metal atoms. The photogenerated electrons can be trapped in Ti³⁺, thereby preventing the recombination of the majority and minority carriers. Moreover, Ti³⁺ formation is related to the oxygen vacancies.²³ Therefore, the increased Ti³⁺ of the *d*-TiO₂ NPs indicates that the *d*-TiO₂ NPs have more defects.

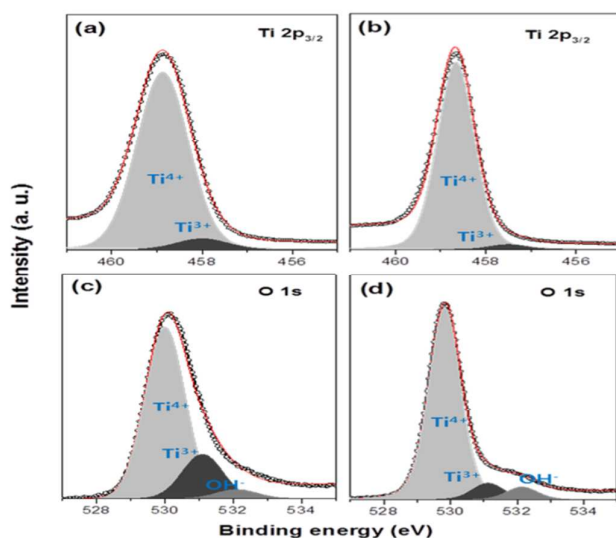


Fig. 6 X-ray photoelectron spectra of Ti 2p ((a) and (b)) and O 1s ((c) and (d)) for *d*-TiO₂ NPs ((a) and (c)) and P25 TiO₂ ((b) and (d))

To test whether the *d*-TiO₂ NPs can readily infiltrate the biological cells, we examined their distribution and sizes in aqueous solution according to the zeta potential and DLS measurements. The zeta potentials of the *d*-TiO₂ NPs and P25 TiO₂ were strongly negatively charged at pH 7.0 in deionized water, at around -22.5 mV and -21.8 mV, respectively (Fig. S2). Such large zeta potential values can affect the distribution of particles. In other words, if particles have a small zeta potential, there is no force to prevent the particles from coming together, leading to their aggregation. Further details of the aggregation of the *d*-TiO₂ NPs and P25 TiO₂ were monitored via particle size measurement using DLS to determine their stability in deionized water (Fig. S3). When dispersed in water at pH = 7.0 at a concentration of 1 mg/mL, the *d*-TiO₂ NPs showed reduced agglomeration (224 nm) compared to that of P25 TiO₂ (1440 nm). These results indicate that the synthesized *d*-TiO₂ NPs can disperse better than P25 TiO₂ in solution. Therefore, the cellular uptake of *d*-TiO₂ NPs is expected to be improved compared to that of P25 TiO₂.^{19,40-41}

Photocatalytic action on cancer cells

To evaluate the photocatalytic action of the *d*-TiO₂ NPs on cancer cells, the viability of HeLa and Hep-G2 cells was measured using the WST method in the presence of various concentrations of TiO₂ NPs under visible light irradiation. The confocal DIC images of HeLa showed that the addition of the P25 TiO₂ and exposure to visible light caused negligible stress (Fig. 7). Similar cell morphology was observed when HeLa cells were treated with and without the P25 TiO₂ in dark and under visible light, indicating no major effect of either visible light or the P25 TiO₂ on cell viability. In contrast, upon visible light irradiation with *d*-TiO₂ NPs, the HeLa cells showed extensive cell death (about 70%, as estimated by cell counting).

These observations were confirmed more quantitatively by the cell viability measurements using the WST method (Fig. 8 (A)). In the dark, the viabilities of both HeLa and Hep-G2 cells remained strong, at over 90%, with the treatment of 25 µg/mL *d*-TiO₂ NPs and P25 TiO₂. Over 80% of the cells in both cell lines also survived under visible light irradiation

without TiO₂ NPs. In the dark, the cell viabilities remained the same when treated with much higher concentrations of TiO₂ NPs, up to 100 μg/mL as shown in Fig. 8 (B) and (C). However, under visible-light irradiation with TiO₂ NPs, the viabilities of both HeLa and Hep-G2 cells decreased to 30% and 40%, respectively; their viabilities further decreased with increasing TiO₂ NPs concentrations. This indicates that TiO₂ NPs photocatalyze the killing of cancer cells under visible light. In particular, the minimum concentrations of the *d*-TiO₂ NPs required to observe the photocatalytic killing of HeLa and Hep-G2 cells (70 % and 60 % death rates, respectively) were much lower (25 μg/mL and 50 μg/mL) than those of P25 TiO₂, implying that the visible-light photocatalytic effect of the *d*-TiO₂ NPs is much stronger than that of P25 TiO₂. The difference in the concentration dependence of the photocatalytic-killing effect between HeLa and Hep-G2 cells may also imply that HeLa cells can uptake *d*-TiO₂ NPs more easily than Hep-G2 cells. Recently Li *et al.*¹² demonstrated the visible-light photocatalytic killing of HeLa cells up to 60% using N-doped TiO₂ NPs at a concentration of 200 μg/mL which is eight times higher than concentration used in our study under the same illumination condition. This comparison suggests that the visible-light photocatalytic activity of *d*-TiO₂ NPs in the killing of cancer cells is much more effective than that of N-doped TiO₂ NPs.

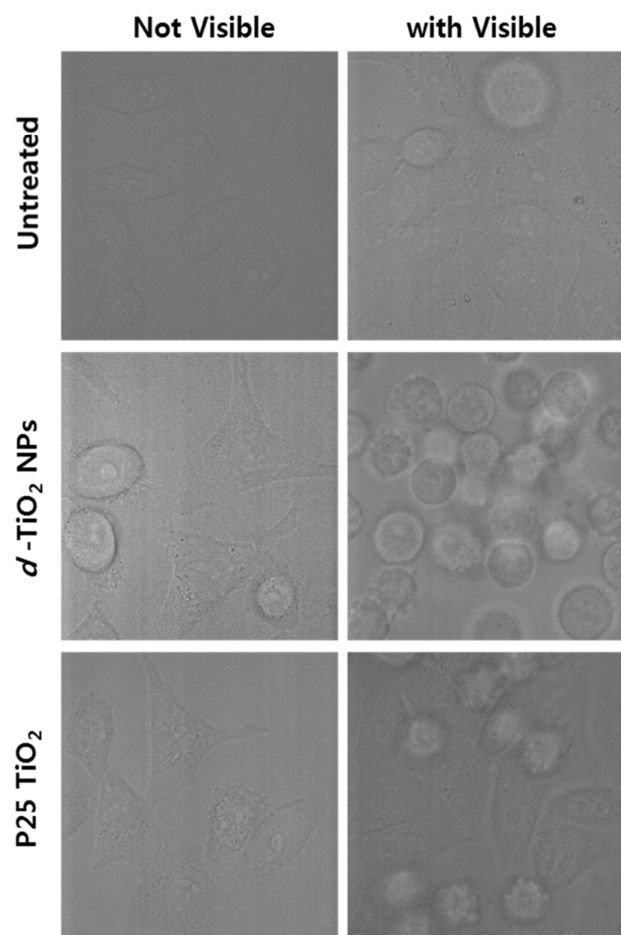
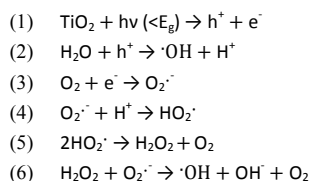


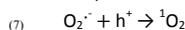
Fig. 7 Confocal DIC images of HeLa cells without or with *d*-TiO₂ NPs (or P25 TiO₂) under visible light irradiation or in the dark.

In general, it is known that the photocatalytic action of TiO₂ NPs on cancer cells is mostly triggered by the photoinduced generation of various reactive oxygen species (ROS) such as hydroxyl radicals ($\cdot\text{OH}$), hydrogen peroxide (H₂O₂), and superoxide anion radicals (O₂^{·-}) on the surface of cell membranes and in the cytoplasm.^{9,25,40} This occurs because TiO₂ NPs can attach to the cellular membranes and enter the cytoplasm via endocytosis.^{37,41} From this perspective, the *d*-TiO₂ NPs are also expected to generate ROS in cancer cells upon visible light irradiation, as shown in the following equations:



The *d*-TiO₂ NPs absorb the visible light with energy larger than the band gap. Band gap excitation of the *d*-TiO₂ NPs results in e⁻(conduction band) – h⁺ (valence band) separation. The high oxidative potential of the holes allows the formation of reactive intermediates such as H⁺ and $\cdot\text{OH}$. The reactive $\cdot\text{OH}$ can be formed by the decomposition of water. Meanwhile, the electrons are usually reactive with O₂ to yield O₂^{·-}. Moreover, some HO₂[·] can form H₂O₂, and the reaction of H₂O₂ can also result in the formation of $\cdot\text{OH}$.

In addition to conventional ROS, it was recently reported that TiO₂ NPs can efficiently generate ¹O₂ by energy transfer *via* the defect sites if they absorb long-wavelength visible light and NIR wavelengths (700-1000 nm) in addition to an electron transfer mechanism (Nosaka's mechanism),²⁴ as shown in the next equation.



Since the *d*-TiO₂ NPs were shown to absorb long-wavelength visible

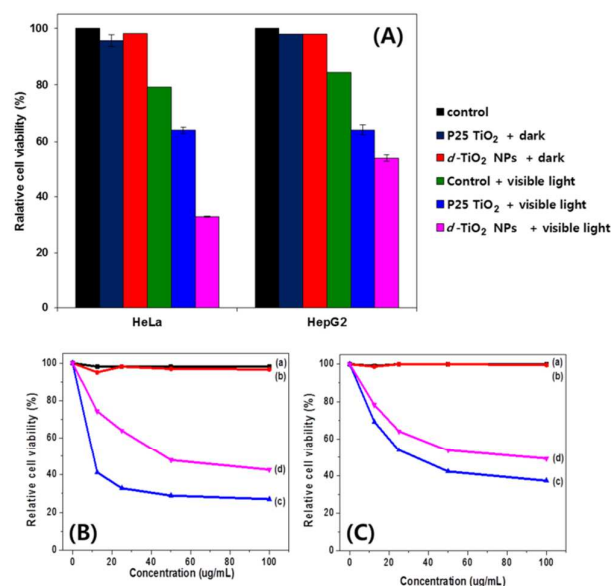


Fig. 8 (A) Histogram of the photokilling effects of TiO₂ (25 μg/mL) on the relative viabilities of HeLa and Hep-G2 cells under visible light irradiation or in the dark. Relative cell viabilities as a function of TiO₂ NP concentrations for HeLa (B) and Hep-G2 (C) cells in dark ((a) and (b)) and under visible light irradiation ((c) and (d)) with *d*-TiO₂ NPs ((a) and (c)) and P25 TiO₂ ((b) and (d)).

light and NIR light, we attempted to confirm the photoinduced formation of $^1\text{O}_2$ by using the SOSG reagent.²⁸⁻²⁹ SOSG is highly selective in reactions with $^1\text{O}_2$, without any appreciable response to $\cdot\text{OH}$ or $\cdot\text{O}_2^-$. This indicator initially exhibits weak fluorescence; however, in the presence of $^1\text{O}_2$, it emits strong fluorescence. Fig. 9 (C) shows a plot of the SOSG fluorescence intensity measured at 529 nm with *d*-TiO₂ NPs (a) or P25 TiO₂ (b), depending on the visible-light (460–800 nm) irradiation time. The fluorescence intensity of SOSG with *d*-TiO₂ NPs was higher than that observed with P25 TiO₂, indicating that the *d*-TiO₂ NPs generate $^1\text{O}_2$ via their defect sites. Therefore, it can be concluded that the *d*-TiO₂ NPs may show enhanced photocatalytic killing of cancer cells owing to the generation of $^1\text{O}_2$ in addition to the other ROS in the photooxidation of cell components. This potential mechanism is summarized in a schematic shown in Fig. 10.⁴² These results suggest that the *d*-TiO₂ NPs are promising materials for future *in vivo* PDT of cancer cells under long-wavelength visible and NIR light irradiation.

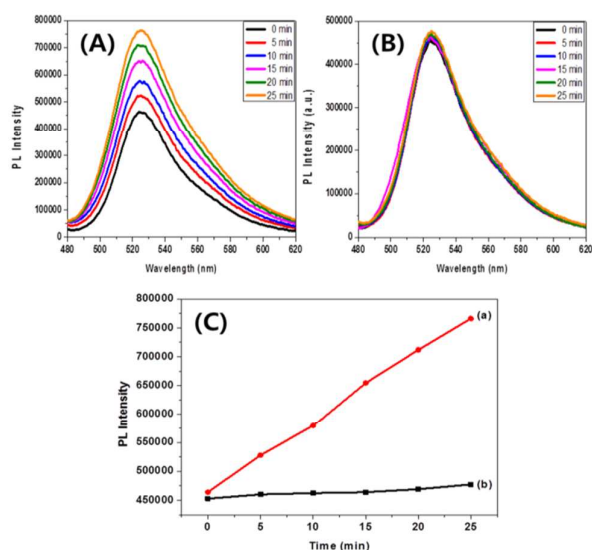


Fig. 9 Fluorescence intensity of aqueous SOSG measured at the maximum of 529 nm upon excitation at 480 nm in the presence of or *d*-TiO₂ NPs (A) or P25 TiO₂ (B) after visible light irradiation by a xenon lamp. (C) Fluorescence intensity of the aqueous SOSG solution in the presence of *d*-TiO₂ NPs (a) or P25 TiO₂ (b) over time.

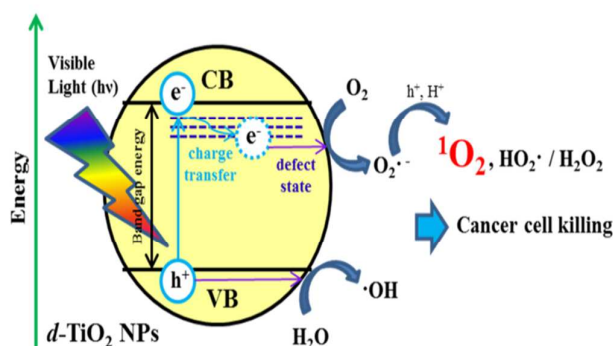


Fig. 10 Schematic of the mechanism for the photokilling of cancer cells by the *d*-TiO₂ NPs.

Experimental section

Chemicals

All of the chemicals used for the synthesis of *d*-TiO₂ NPs, including P-25 (Degussa-Huls), egg lecithin (L-R-phosphatidylcholine, >60%, Sigma-Aldrich), chloroform (>99.8%, Samchun, Korea), sodium hydroxide (>93%, Duksan, Korea), and ethanol (200-proof, >99.8%, Sigma-Aldrich), were of analytical grade and used without further purification.

Synthesis of *d*-TiO₂ NPs

The *d*-TiO₂ NPs were synthesized by the combination of sol-gel and hydrothermal reactions through the formation of liposome-TiO₂ composites.²⁶ A schematic representation of the synthesis procedure is shown in Fig. 1. Initially, the precursor solution was prepared by adding 50 mL of a 1.0 M NaOH aqueous solution into 0.1 g of P-25 powder in an ethanol (30 mL) mixture at room temperature under constant stirring. To prepare the liposome-TiO₂ composites, thin phospholipid films were prepared by evaporating a chloroform solution of egg lecithin lipid to dryness in a round-bottomed flask under reduced pressure. The lipid films were mixed with a precursor solution, followed by sonication for 30 min in an ultrasonic bath (Fisher Scientific model FS20, 70 W, 42 kHz) until the turbid liposome-TiO₂ composites were formed. The turbid solution of the liposome-TiO₂ composites was transferred into a Teflon-lined stainless steel autoclave and maintained at 180 °C for 24 h for the hydrothermal reaction. After the hydrothermal reaction, the autoclave was cooled naturally to room temperature. The solid matter was then collected and washed in distilled water and ethanol several times, followed by calcinations at 823 K for 24 h to form NPs.

Structural and optical characterization

The crystallinity and structure of the as-prepared NPs were characterized by X-ray diffraction (XRD) using a rotating anode X-ray diffractometer (D/MAX-2200 Ultima/PC) with CuK α radiation (λ : 1.5405 Å). The crystalline phases and functional groups of the samples were also determined by Raman spectroscopy (Lab RAM HR-800, Horiba Jobin Yvon). The vibrational structures of the *d*-TiO₂ NPs were investigated using Fourier transform-infrared (FT-IR) spectroscopic analysis; the FT-IR spectra were recorded with the KBr pellet technique using a JASCO FT-IR 4100 spectrometer. The size and morphology of the synthesized *d*-TiO₂ NPs were examined by transmission electron microscopy (TEM; Tecnai G2 F30). The TEM sample was prepared by dip-coating Formvar/carbon film-Cu grids with a nanocolloidal solution obtained by sonication of the synthesized *d*-TiO₂ NPs in ethanol.

To evaluate the absorptions of the synthesized *d*-TiO₂ NPs in the visible-light region, diffuse reflectance UV-VIS-NIR absorption spectra (DRS) were recorded on a Solid Spec-3700 double-beam spectrophotometer equipped with an integrating sphere. The steady-state fluorescence spectra were obtained at room temperature with a PL spectrometer at 325 nm (Lab RAM HR-800, Horiba Jobin Yvon). X-ray photoelectron spectra (XPS) were obtained using monochromatic Al K α X-ray radiation (1486.6 eV) with a power of 120 W (Kratos Analytical, AXIS Nova, UK).

The particle sizes and zeta potentials of the dispersed solution of the *d*-TiO₂ NPs and P25 TiO₂ were measured by dynamic light scattering (DLS) and laser Doppler velocimetry (LDV), respectively, using an electrophoretic light scattering spectrophotometer (Otsuka Electronics Co, Ltd; ELS-Z2). Confocal differential interference contrast (DIC) images of HeLa cells with or without the *d*-TiO₂ NPs and visible

light irradiation were observed by laser-scanning confocal microscopy (LSCM; LSM5 live configuration Vario Two VRGB).

Cell culture

The human cervical carcinoma cells (HeLa) and human hepatocellular carcinoma cells (Hep-G2) were grown in 89% Dulbecco's modified Eagle's medium with 10% fetal bovine serum and 1% antibiotic-antimycotic solution. The cells were routinely maintained in the plastic tissue culture dishes at 37 °C under a humidified 5% CO₂-containing atmosphere.

Evaluation of cytotoxicity

The cytotoxicity of the injected TiO₂ NPs was evaluated using the EZ-Cytox reagent (Daeil Lab Service, Seoul, South Korea) based on the water-soluble tetrazolium (WST) method.²⁷ HeLa or Hep-G2 cells were seeded at a density of 1.5×10^4 cells per well in a 96-well microassay plate, and incubated for 24 h at 37 °C under a 5% CO₂ atmosphere. The *d*-TiO₂ NPs or P25 TiO₂ were added to the incubated cells at various concentrations, followed by further incubation for additional 24 h at 37 °C. Next, 10 μL of the EZ-Cytox reagent was added and the plates were incubated for 2 h at 37 °C. The absorbance of the EZ-Cytox reagent was measured at 450 nm using a microplate reader (VersaMax, Molecular Devices, USA). The cell viability (%) was calculated using the following equation: cell viability (%) = (OD_{450(sample)} / OD_{450(control)}) × 100.

Photocatalytic killing of cancer cells

The cancer cells incubated with different concentration of the *d*-TiO₂ NPs or P25 TiO₂ were irradiated for 4 h with the visible light emitted from a 300-W xenon lamp (Asahi Spectra, Japan). The 400 nm long-pass filter (GG 400) and heat-absorbing colored glass filter (KG 5) were used to cut off the UV and far-infrared wavelengths, respectively. All filters were purchased from Newport, USA. The visible-light power density at the liquid surface in the cell wells was 12 mW/cm², as measured by a power meter (model 2936-C, Newport, USA). The irradiated cancer cells were incubated in the dark for another 24 h before analyzing the cell viability as described above.

Determination of singlet oxygen generation from TiO₂ NPs

Singlet oxygen (¹O₂) generation was monitored by using the singlet oxygen sensor green (SOSG) reagent.²⁸⁻²⁹ Stock solutions of 5 mM SOSG were dissolved in methanol/water (3:97 v/v) to obtain a final concentration of approximately 1 μM. Subsequently, a 10 μM solution of *d*-TiO₂ NPs (or P25 TiO₂) was added to the 1 μM SOSG solution under stirring. This sample was irradiated under the visible-light region with a xenon lamp (Asahi Spectra; MAX-302) and a 460 nm long-pass filter every 5 min, followed by measuring the SOSG fluorescence changes (500-600 nm) upon excitation at 480 nm.

Conclusions

The defective TiO₂ nanoparticles (*d*-TiO₂ NPs) were synthesized using a simple hydrothermal gel/sol technique from P25 TiO₂ powder. Using various spectroscopic, diffraction, and microscopic techniques, we compared the structural properties and morphology of the *d*-TiO₂ NPs to P25 TiO₂. Absorbance at long wavelengths, including NIR, was confirmed, and agglomeration was reduced (~224 nm) compared to that of P25 TiO₂ (~1440 nm) in aqueous solution, indicating that the *d*-TiO₂ NPs could infiltrate the cell membrane to access cancer cells. The improved cell-killing effect of the *d*-TiO₂ NPs in two cancer cell lines was confirmed, which was triggered by long-wavelength visible light to generate reactive oxygen species including

singlet oxygen (¹O₂). Thus, *d*-TiO₂ NPs show good potential for novel photodynamic therapy strategies in cancer treatment.

Acknowledgements

This work was supported in part by the National Research Foundation of Korea (Project number: NRF 2012R1A1A 2039168) and by the Korea Basic Science Institute Grant D35500.

Notes and references

1. L. Wang, Y. Liu, W. Li, X. Jiang, Y. Ji and X. Wu, L. Xu, Y. Qiu, K. Zhao, T. Wi, Y. Li, Y. Zhao and C. Chen, *Nano Lett.*, 2011, **11**, 772-780.
2. K. T. Thurn, E. M. B. Brown, A. Wu, S. Vogt, B. Lai, J. Maser, T. Paunesku and G. E. Woloschak, *Nanoscale Res Lett.*, 2007, **2**, 430-441.
3. S. Jiang, M. K. Gnanasammandhan and Y. Zhang, *J. R. Soc. Interface.*, 2010, **7**, 3-18.
4. R. K. Visaria, R. J. Griffin, B. W. Williams, E. S. Ebbini, G. F. Paciotti, C. W. Song and J. C. Bischof, *Mol. Cancer Ther.*, 2006, **5**, 1014-1020.
5. Z. F. Yin, L. Wu, H. G. Yang and Y. H. Su, *Phys. Chem. Chem. Phys.*, 2013, **15**, 4844-4858.
6. K. Sunada, T. Watanabe and K. Hashimoto, *J. Photochem. Photobiol., A*, 2003, **156**, 227-233.
7. M. Kalbacova, J. M. Macak, F. Schmidt-Stein, C. T. Mierke and P. Schmuki, *Phys. Stat. Sol.*, 2008, **2**, 194-196.
8. A. Zhang and Y. Sun, *World J. Gastroent.*, 2004, **10**, 3191-3193.
9. K. Matsui, M. Karasaki, M. Segawa, S. Y. Hwang, T. Tanaka, C. Ogino and A. Kondo, *Med. Chem. Commun.*, 2010, **1**, 209-211.
10. S. Zhang, D. Yang, D. Jing, H. Liu, L. Liu, Y. Jia, M. Gao, L. Guo and Z. Huo, *Nano Res.*, 2014, **7**, 1659-1669.
11. A. B. Ormond and H. S. Freeman, *Materials*, 2013, **6**, 817-840.
12. Z. Li, L. Mi, P. Wang and J. Chen, *Nanoscale Res. Lett.*, 2011, **6**, 356-362.
13. Z. Li, X. Pan, T. Wang, P. N. Wang, J. Y. Chen and L. Mi, *Nanoscale Res. Lett.*, 2013, **8**, 96-102.
14. A. Yu, G. Wu, F. Zhang, Y. Yang and N. Guan, *Catal Lett*, 2009, **129**, 507-512.
15. L. Liu, P. Miao, Y. Xu, Z. Tian, Z. Zou and G. Li, *J. Photochem. Photobiol. B*, 2010, **98**, 207-210.
16. A. Md, K. Yoshihumi and S. Md, *J. Mater. Chem.*, 2012, **22**, 5460-5469.
17. K. Huang, L. Chen, J. Deng and J. Xiong, *J. Nanomater.*, 2012, **2012**, 720491-720502.
18. S. L. Jacques, *Phys. Med. Biol.*, 2013, **58**, 37-61.
19. L. K. Braydich-Stolle, N. M. Schaublin, R. C. Murdock, J. Jiang, P. Biswas, J. J. Schlager and S. M. Hussain, *J. Nanopart. Res.*, 2009, **11**, 1361-1374.
20. M. M. Khan, S. A. Ansari, D. Pradhan, M. O. Ansari, D. H. Han, J. Lee and M. H. Cho, *J. Mater. Chem. A*, 2014, **2**, 637-644.
21. S. Latthe, S. An, S. Jin and S. Yoon, *J. Mater. Chem. A*, 2013, **1**, 13567-13575.
22. M. S. Kim, W. J. Jo, D. Lee, S. Baek, J. H. Shin and B. C. Lee, *Bull. Kor. Chem. Soc.*, 2013, **34**, 1397-1400.
23. X. Pan, M. Yang, X. Fu, N. Zhang and Y. Xu, *Nanoscale*, 2013, **5**, 3601-3614.
24. M. Buchalska, P. Labuz, L. Bujak, G. Szweczyk, T. Sarna, S. Mackowski and W. Macyk, *Dalton Trans.*, 2013, **42**, 9468-9475.
25. H. Shi, R. Magaye, V. Castranova and J. Zhao, *Part. Fibre Toxicol.*, 2013, **10**, 15-47.
26. J. Lee and M. Yoon, *J. Phys. Chem. C*, 2009, **113**, 11952-11958.
27. V. Balakrishnan, H. A. A. Wab, K. A. Razak and S. Shamsuddin, *J. Nanomater.*, 2013, **2013**, 729306-729313.
28. A. Gollmer, J. Arnbjerg, F. H. Blaikie, B. W. Pedersen, T. Breitenbach, K. Daasbjerg, M. Glasius and P. R. Ogilby, *J. Photochem. Photobiol.*, 2011, **87**, 671-679.
29. Y. Shen, H. Y. Lin, Z. F. Huang, D. F. Chen, B. H. Li and S. S. Xie, *Laser Phys. Lett.*, 2011, **8**, 232-238.
30. J. Yu, H. Yu, B. Cheng, M. Zhou and X. Zhao, *J. Mol. Catal. A: Chem.*, 2006, **253**, 112-118.

31. R. Carrer-Lopez and S. Castillo-Cervantes, *Superficies y Vacio*, 2012, **25**, 82-87.
32. M. J. Kim, K. D. Kim, W. S. Tai, H. O. Seo, Y. Luo, Y. D. Kim, B. C. Lee and O. K. Park, *Catal. Lett.*, 2010, **135**, 57-61.
33. X. Chen, Y. Lou, A. C. S. Samia, C. Burda and J. L. Gole, *Adv. Funct. Mater.*, 2005, **15**, 41-49
34. M. Yoon, M. Seo, C. Jeong, J. H. Jang and K. S. Jeon, *Chem. Mater.* 2005, **17**, 6069-6079.
35. P. A. Dokhale, N.D. Sali, P. Madhu Kumar, S. V. Bhoraskar, V. K. Rohatgi, V. N. Bhoraskar, S. K. Date and S. Badrinarayanan, *Mater. Sci. Eng.*, 1997, **49**, 18-26.
36. G. Liu, C. Han, M. Pelaez, D. Zhu, S. Liao, V. Likodimos, N. Ioannidis, A. G. Kontos, P. Falaras, P. S. M. Dunlop, J. A. Byrne and D. D. Dionysiou, *Nanotechnology*, 2012, **23**, 294003-294013.
37. J. Lee, J. S. Choi and M. Yoon, *J. Mater. Chem. B*, 2014, **2**, 2133-2317
38. S. Kalathil, M. M. Khan, S. A. Ansari, J. Lee and M. H. Cho, *Nanoscale*, 2013, **5**, 6323-6326.
39. M. Kong, Y. Li, X. Chen, T. Tian, P. Fang, F. Zheng and X. Zhao, *J. Am. Chem. Soc.*, 2011, **133**, 16414-16417.
40. M. J. Akhtar, M. Ahamed, S. Kumar, M. A. M. Khan, J. Ahmad and S. A. Alrokayan, *Intern. J. Nanomed.*, 2012, **7**, 845-857.
41. T. Iversen, T. Skotland and K. Sandvig, *Nano Today*, 2011, **6**, 176-185.
42. Y. Li, W. Zhang, J. Niu and Y. Chen, *ACS NANO*, 2012, **6**, 5164-5173.

Table of Contents

Hydrothermal synthesis of defective TiO₂ nanoparticles for long-wavelength visible light-photocatalytic killing of cancer cells

Jooran Lee, Young Hwa Lee, Joon Sig Choi, Kwan

Seob Park, Ki Soo Chang* and Minjoong Yoon*

Newly fabricated *d*-TiO₂ NPs were demonstrated to be efficient in long wavelength visible light-triggered killing of cancer cells.

